J. Am. Soc. Mass Spectrom. (2018) 29:1231–1241
DOI: 10.1007/s13361-018-1927-9

FOCUS: MASS SPECTROMETRY IN GLYCOBIOLOGY AND RELATED FIELDS: RESEARCH ARTICLE

Tandem Mass Spectrometry and Ion Mobility Reveals Structural Insight into Eicosanoid Product Ion Formation

James P. Di Giovanni, Robert M. Barkley, David N. M. Jones, Joseph A. Hankin, Robert C. Murphy

Department of Pharmacology, University of Colorado Denver, Mail Stop 8303, 12801 E. 17th Ave, Aurora, CO 80045, USA

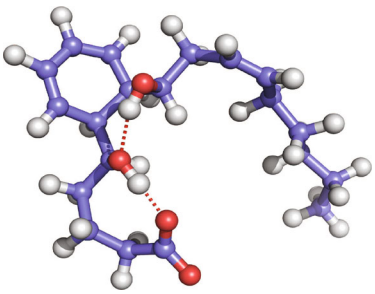

Leukotriene B_4 [M-H]$^-$

Abstract. Ion mobility measurements of product ions were used to characterize the collisional cross section (CCS) of various complex lipid [M-H]$^-$ ions using traveling wave ion mobility mass spectrometry (TWIMS). TWIMS analysis of various product ions derived after collisional activation of mono- and dihydroxy arachidonate metabolites was found to be more complex than the analysis of intact molecular ions and provided some insight into molecular mechanisms involved in product ion formation. The CCS observed for the molecular ion [M-H]$^-$ and certain product ions were consistent with a folded ion structure, the latter predicted by the proposed mechanisms of product ion formation. Unexpectedly, product ions from [M-H-H_2O-CO_2]$^-$ and [M-H-H_2O]$^-$ displayed complex ion mobility profiles suggesting multiple mechanisms of ion formation. The [M-H-H_2O]$^-$ ion from LTB_4 was studied in more detail using both nitrogen and helium as the drift gas in the ion mobility cell. One population of [M-H-H_2O]$^-$ product ions from LTB_4 was consistent with formation of covalent ring structures, while the ions displaying a higher CCS were consistent with a more open-chain structure. Using molecular dynamics and theoretical CCS calculations, energy minimized structures of those product ions with the open-chain structures were found to have a higher CCS than a folded molecular ion structure. The measurement of product ion mobility can be an additional and unique signature of eicosanoids measured by LC-MS/MS techniques.

Keywords: Ion mobility, Eicosanoids, TWIMS, Mechanism, Product ions, Molecular dynamics calculations, CCS calculation, Hydroxy, polyunsaturated fatty acids, Lipids

Received: 14 December 2017/Revised: 23 February 2018/Accepted: 23 February 2018/Published Online: 23 April 2018

Introduction

Metabolites of arachidonic acid play significant roles in biology serving as lipid mediators of cellular activation [1]. They perform this action as a result of complex biochemical conversion orchestrated into oxygenated 20-carbon fatty acids catalyzed by prostaglandin H synthase [2], 5-lipoxygenase [3], 15-lipoxygenase, 12-lipoxygenase as well as various isoforms of cytochrome P450 [4, 5]. Once synthesized inside the cell at intracellular membrane sites, the eicosanoids are released into the extracellular medium. The unique lipid structures of the various eicosanoid mediators can then be recognized by specific cell-surface protein receptors expressed by cells in the local tissue environment, which are linked to G-protein-mediated signaling events within the responding cell. Mass spectrometry was widely used to qualitatively identify these complex lipids that are made in response to stimulation of the cell that expresses the prostaglandin H synthase or

Electronic supplementary material The online version of this article (https://doi.org/10.1007/s13361-018-1927-9) contains supplementary material, which is available to authorized users.

Correspondence to: Robert Murphy; *e-mail:* Robert.Murphy@ucdenver.edu

regiospecific lipoxygenases as well as a preferred method to quantitate their production in biological fluids using stable isotope dilution techniques [6].

Analysis of lipids by tandem mass spectrometry after electrospray ionization and reverse phase liquid chromatography was an extraordinarily powerful means to carry out both specific identification and quantitation in complex mixtures that are observed in biological extracts [7]. Recently, ion mobility emerged as a powerful means to increase the power of such mass spectrometric techniques that can further drive an increase in sensitivity and specificity in the analysis of lipids with emphasis on phospholipids [8–11]. Various forms of ion mobility including high-field asymmetric wave form ion mobility (FAIMES) [12, 13], uniform field drift cell ion mobility [14], and traveling wave ion mobility [15] (TWIMS) became commercially available and are nicely suited for the analysis of fatty acids [16], phospholipids [8, 17], neutral lipids [18], and sphingolipids [19] as well as eicosanoids [20].

Most studies of ion mobility-based mass spectrometry of lipids employed ion mobility of the precursor ion such as $[M-H]^-$ of fatty acids and eicosanoids or $[M+H]^+$ of complex lipids such as phospholipids, sphingolipids, and neutral lipids. Recently, we reported an interesting advantage in employing ion mobility measurements of product ions as a means to rapidly identify lipids in complex mixtures [18, 21]. We applied this strategy to the analysis of eicosanoids but found that certain product ions from specific eicosanoids behaved in an unexpected manner with complex ion mobility profiles that suggest populations of alternative structures for these product ions. These observations served as the basis of a study of this phenomenon and molecular calculations of ion structure.

Experimental

Materials Eicosanoid standards (leukotriene B_4, prostaglandin E_2, 5-hydroxy-6,8,11,14-eicosatetraenoic acid, 8-hydroxy-5,9,11,14-eicosatetraenoic acid, 9-hydroxy-5,7,11,14-eicosatetraenoic acid, 11-hydroxy-5,8,12,14-eicosatetraenoic acid, 12-hydroxy-5,8,10,14-eicosatetraenoic acid, 15-hydroxy-6,8,11,13-eicosatetraenoic acid), LTB_4 and LTA_4 methyl ester were purchased from Cayman Chemical (Ann Arbor, MI). Solvents and chemicals used for liquid chromatography were HPLC grade, purchased from Fisher Scientific Company (Pittsburgh, PA).

5-Hydroxy-12-[^{18}O] Hydroxy-6,8,11,14-Eicosatetraenoic Acid Isotopically labeled 6-trans LTB_4 was prepared by acid catalyzed Michael addition of $H_2{}^{18}O$ (Rotem Industries Ltd., Israel, 98 atom % excess) at C-12 of the LTA_4 methyl ester prior to saponification of the ester. LTA_4 methyl ester (1 μg) in hexanes was dried in a glass test tube under a stream of dry N_2 gas. To this was added 40 μL acetone, 10 μL $H_2{}^{18}O$, and 0.5 mg benzoic acid. The mixture was vortexed and set in a heating block at 37 °C for 30 min. Saponification was carried out with further addition of 40 μL acetone and 10 μL 0.5 M NaOH in H_2O. The mixture was vortexed and allowed to set for 25 °C for 60 min. The mixture was dried under a stream of dry nitrogen, followed by addition of 100 μL acetone to extract the organic fraction from residual salts. This was repeated; extracts were combined, dried, and then redissolved in methanol for mass spectrometric analysis.

Mass Spectrometry Mass spectrometry and ion mobility measurements obtained were carried out using a Synapt G2-S instrument (Waters, Manchester, UK) in the negative-ion mode (tandem quadrupole time of flight mass spectrometer with capability for traveling wave ion mobility separations). Mass spectrometer parameters included the following: ESI voltage 2500 V, sampling cone 50 V, source offset 80 V, source temperature 120 °C, desolvation temperature 150 °C, cone gas 10 L/h, desolvation gas 500 L/h, nebulizer 6.0 bar, ion mobility wave height 20 V, and ion mobility wave velocity 220 m/s. Collision induced dissociation was carried out with argon as the collision gas and a collision energy of either 20, 25, or 30 V as indicated. The experiments were carried out in "high resolution" mode.

CCS Calculations The ion mobility times of lipid precursor and product ions were experimentally determined at an ion mobility wave height 20 V, ion mobility wave velocity 220 m/s, and with nitrogen as the ion mobility gas. The centroided ion mobility times were converted into CCS as previously published [22] using polyalanine (20 ng/μL) as a calibrant infused at 20 μL/min. and are expressed in square Angstroms ($Å^2$). In order to determine the reproducibility of the CCS calculations, the ion mobility of LTB_4 $[M-H]^-$ was separately determined over a 6-month period. The polyalanine calibration was run at each of these time points, to independently generate a CCS calibration equation. The $[M-H]^-$ from LTB_4 was found to have an average CCS of 182.6 ± 1.3 $Å^2$ (SD). Additional ion mobility measurements were carried out for LTB_4 using helium as drift gas. The usual inlet gas lines to both the helium cell and nitrogen to the IMS cell of the Synapt G2-S were fixed with tee-fittings and shut-off valves so that N_2 could be replaced with He in the IMS cell. The usual flow settings, 180 mL/min in the helium cell and 90 mL/min in the IMS cell, were maintained and other parameters adjusted as previously published [23].

Molecular Dynamics and Theoretical Collisional Cross Section

Molecular dynamics calculations for each potential ion species were performed using Chimera. Three-dimensional structures for each ion were generated using Marvin 5.9.4 (ChemAxon: (http://www.chemaxon.com) and partial charges were assigned using the semi empirical AM1-BCC force field [1] in UCSF Chimera 1.13 [24]. Structure was energy minimized with 1000 steps of steepest descent minimization followed by 100 steps of conjugate gradient minimization. Each structure was then equilibrated to 298 K for 10,000 steps with velocity rescaling followed by, on average, 3 ns steps of dynamics at 298 K using

a 1 fs time step. All calculations were performed using the MMTK [25] molecular dynamics modules implemented within Chimera [26]. The resulting molecular dynamics trajectories showed that almost all ions tested completely sampled the complete range of structural states available to the ions during the time course of the simulations. The notable exception was the LTB_4 $[M\text{-}H]^-$ which showed significant stabilization of states involving hydrogen bonds between the C1 carboxylate and the hydroxyl at C5 or C12. For these ions, calculations were repeated multiple times. For each calculation, a series of 20–30 ions was selected to represent the different conformational states present during the simulations. Subsequently, predicted collisional cross sections (CCS) using both nitrogen and helium as carrier gases were calculated using Trajectory methods with a 6-4-12 Lenard-Jones potential using the program IMos version 1.06 (http://www.imospedia.com) [27, 28].

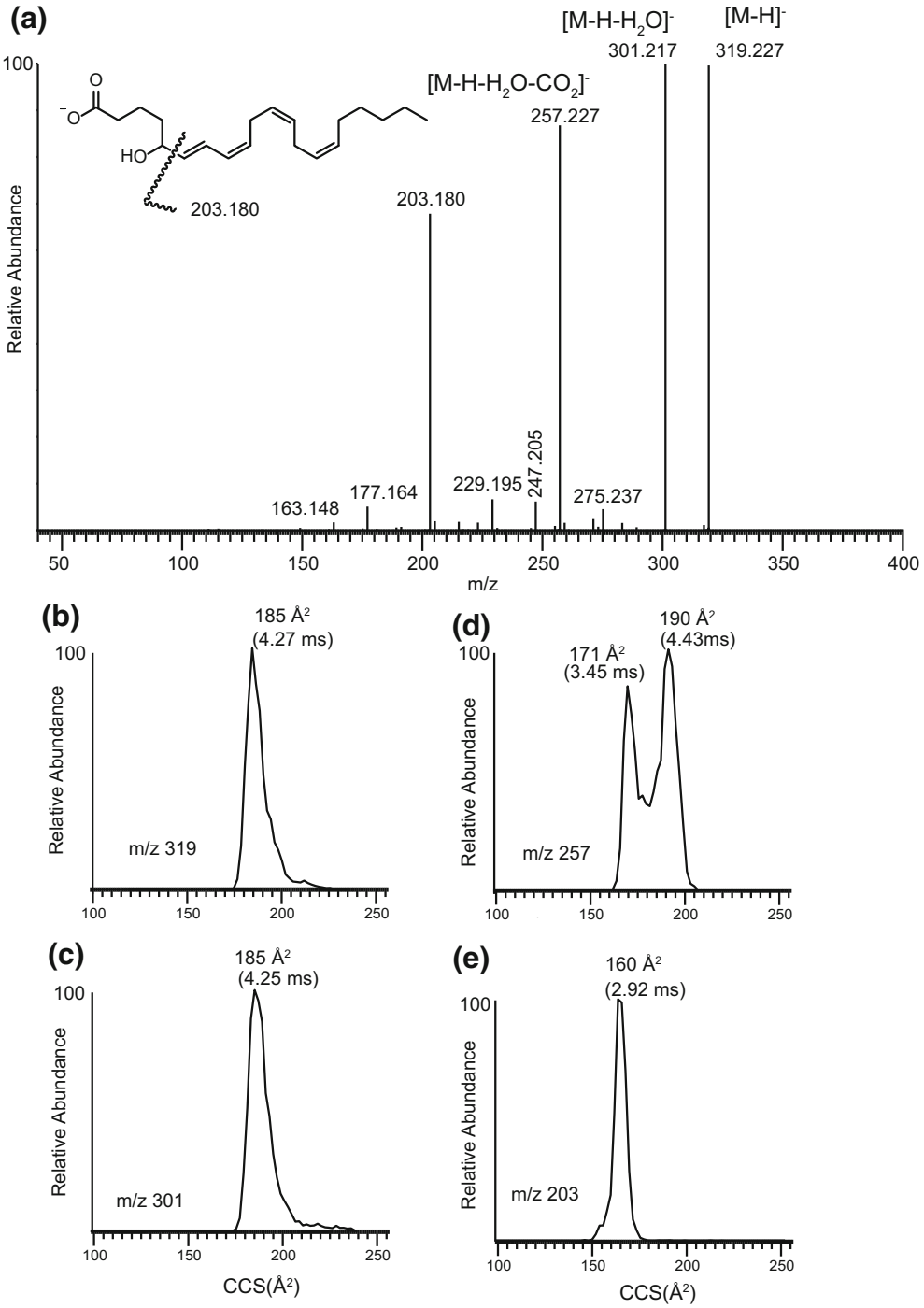

Figure 1. (a) Tandem mass spectrum of 5-HETE. (b) Ion mobility of *m/z* 319.227 $[M\text{-}H]^-$. (c) Ion mobility of *m/z* 301.217 $[M\text{-}H\text{-}H_2O]^-$. (d). Ion mobility of *m/z* 257.227 $[M\text{-}H\text{-}H_2O\text{-}CO_2]^-$. (e) Ion mobility of *m/z* 203.180. See inset structure for origin of *m/z* 203.180

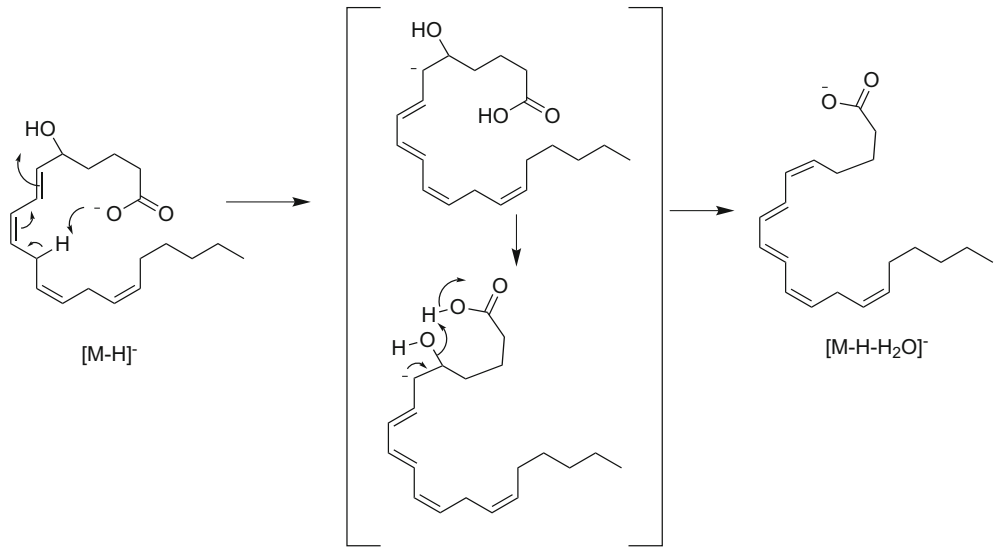

Scheme 1. Collision-induced loss of water from 5-HETE molecular anion

Results and Discussion

Electrospray ionization of hydroxy, unsaturated fatty acids, including eicosanoids, generates $[M-H]^-$ molecular anions that yield abundant product ions after collisional activation [7, 29]. These product ions were studied using various stable isotope-labeled analogs to obtain a picture of the mechanisms for major product ion formation. The most abundant product ions arise from carbon-carbon bond cleavage adjacent to a hydroxyl group for the monohydroxy as well as the dihydroxy eicosanoids [28]. For example, the most abundant product of 5-HETE was suggested to be formal cleavage of the vinylic bond and the carbinol carbon-carbon bond cleavage to form a hydrocarbon ion at *m/z* 203.179 $(C_{15}H_{23})^-$ (Figure 1a). More likely, these cleavage reactions involve either a charge-driven or charge-remote allylic fragmentation processes after a 1[5]-sigmatropic proton shift of the 6,7 double bond and the proton at carbon-13. A charge-driven mechanism was proposed following the carboxyl anion abstracting a proton from the carbon-5 hydroxyl group leading to a charge-driven cleavage of the allylic bond [7]. Thus, inherent in such a mechanism would be folding of the molecule onto itself in order to bring various structural moieties sufficiently close for such unimolecular reactions to occur.

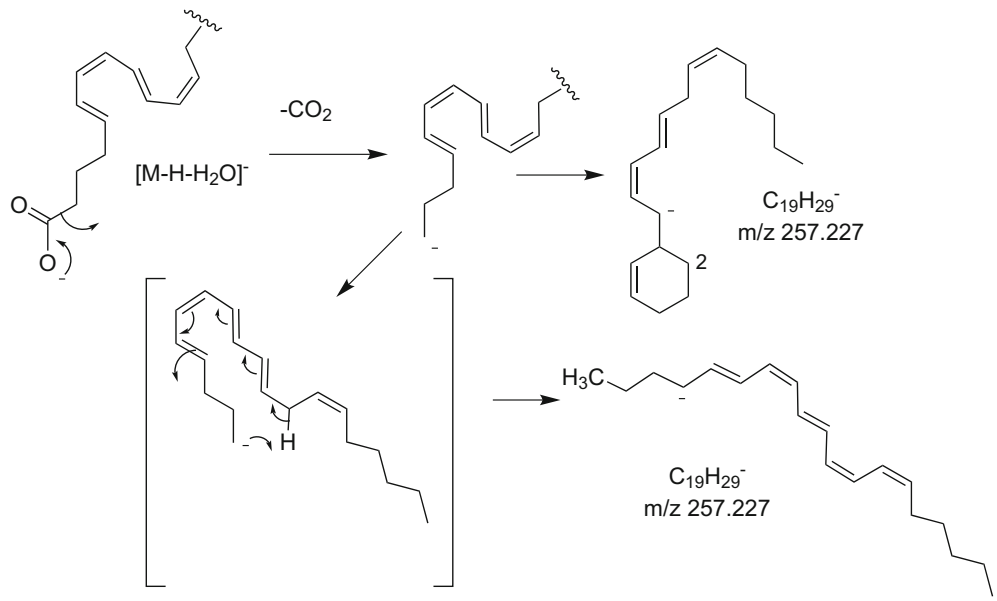

Scheme 2. Collision-induced loss of CO_2 from 5-HETE $[M-H-H_2O]^-$

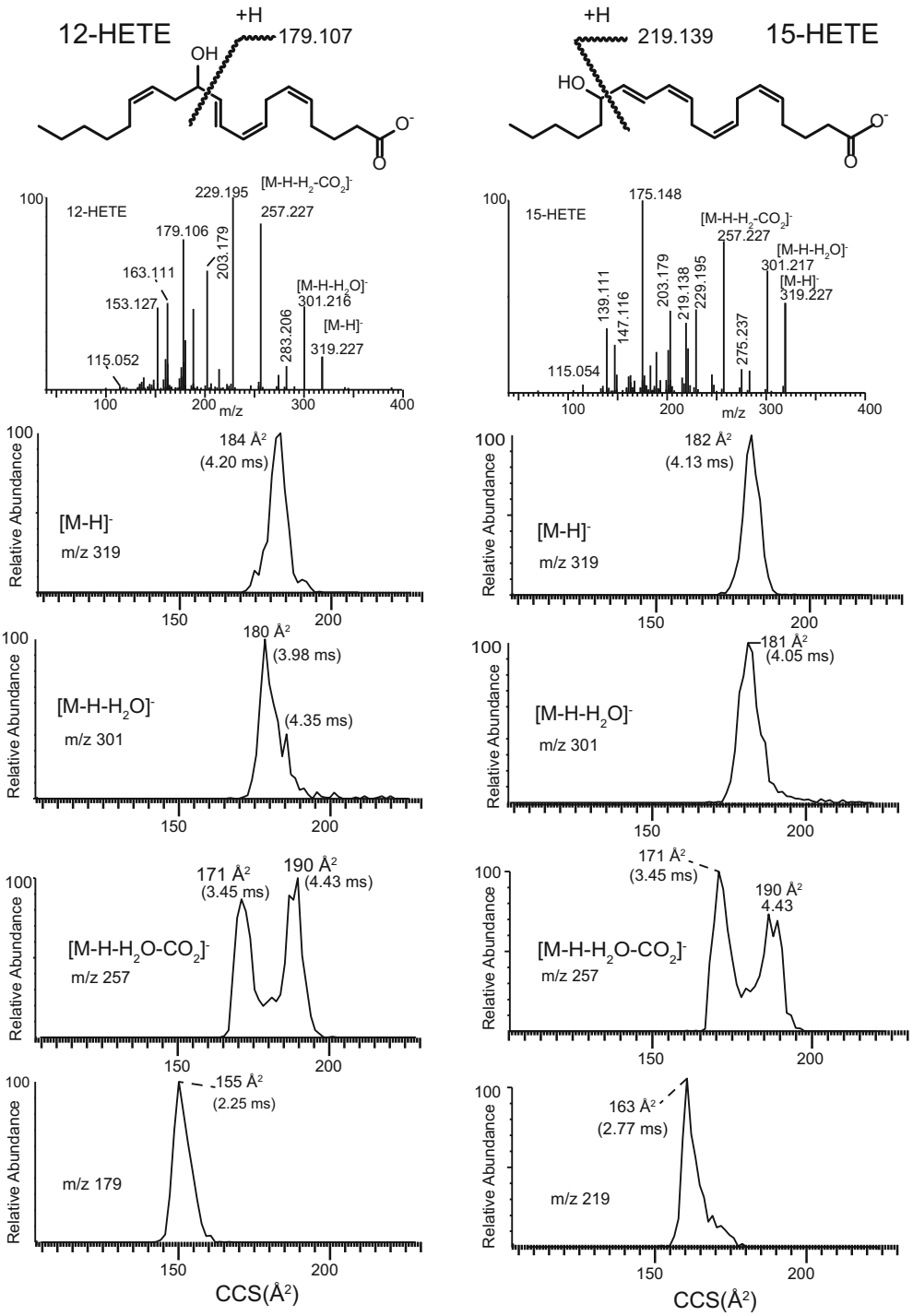

Figure 2. Ion mobility of 12-HETE and 15-HETE for indicated ions $[M-H]^-$, $[M-H-H_2O]^-$, $[M-H-H_2O-CO_2]^-$, and structurally diagnostic allylic cleavage ions for each eicosanoid. See inset structures for origin of *m/z* 179.2 from 12-HETE and *m/z* 219.1 from 15-HETE

Ion mobility profiles derived from 5-HETE $[M-H]^-$ and selected product ions *m/z* 301, 257, and 203 were not all single populations (Figure 1b–e). The ion mobility of the product ion at *m/z* 203 was, as expected, fairly short with a collisional cross section calculated to be 165 Å^2 from a drift time of 2.92 ms whereas the $[M-H]^-$ ion was 185 Å^2 (Figure 1e, b, respectively). Interestingly, there appeared to be at least two populations of ions from the ion mobility profiles of the ion *m/z* 257 $[M-H-H_2O$ and $CO_2]^-$ (Figure 1d). These two quite distinct populations of ions had calculated cross sections 171 and 190 Å^2 respectively. The population of ions of longest drift time had even

higher collisional cross sections than the starting precursor ions $[M-H]^-$ ion at *m/z* 319 (185 Å^2) even though it was 62 Da lower in mass. The two distinct populations of *m/z* 257 suggested two isomeric structures for *m/z* 257 might emanate from the collisional activation of the $[M-H]^-$. The loss of water would appear, at first glance, to be a somewhat trivial loss of a small neutral species, but a charge-driven mechanism could bring a carbon-10 proton close to the carboxylate anion followed by formation of a Δ^5-double bond followed by the loss of H_2O and regeneration of the stabilized carboxylate anion. This loss of a neutral water molecule would then be from a conjugated tetraene $[M-H-H_2O]^-$ (Scheme 1).

Neutral CO_2 could follow from the intermediate formation of the loss of water, possibly in a concerted manner from the dehydrated structure, to form either a cyclic structure or an open-chain, highly conjugated structure (Scheme 2). These two structures would likely have quite distinct ion mobilities. The open-chain form of *m/z* 257 would be expected to have a high collisional cross section (190 Å^2) because the extended conjugated system would be expected to be rather open-chain while the cyclic form of *m/z* 257 would have the lower collisional cross section of 171 Å^2, following the observed trend of folded structures being more highly mobile than unfolded structures [30].

This general trend of two populations of drift times was observed for other hydroxy, polyunsaturated eicosanoids including 12-HETE and 15-HETE (Figure 2) as well as 8-HETE (Supplemental Figure S1), 9-HETE (Supplemental Figure S2), 11-HETE (Supplemental Figure S3), 20-HETE (Supplemental Figure S4) for the loss of CO_2 and H_2O. A single population of ions was observed for $[M-H]^-$ and $[M-H_2O]^-$ and the cleavage ion adjacent to the hydroxyl group at *m/z* 179 and 219 for 12-HETE and 15-HETE, respectively. Even though the loss of CO_2 and H_2O was not very abundant for 11-HETE (Supplemental Figure S3), there was some indication of this trend for two populations of ion mobilities for these ions. This unexpected ion mobility behavior of ions following sequential loss of H_2O and CO_2 for most hydroxy polyunsaturated eicosanoids supported the idea of multiple mechanisms for product ion formation as well as highly folded structures for the precursor ion formed initially by electrospray ionization.

The five hydroxy eicosanoids studied were remarkable in consistency of behavior following collision collisional activation and measurement of collisional cross section of product ions corresponding to the loss of water and water plus CO_2 (Table 1). In spite of the positions of the hydroxyl substituents from carbon-5 to carbon-15, the collisional cross sections for *m/z* 317 and 257 were very similar. This would suggest that interaction of the carboxylate anion with double bonds along the eicosanoid chain, which drives loss of water and forms a stabilized conjugated double bond structure (Scheme 1), occurs relatively easily. Furthermore, the subsequent reactions following the loss of CO_2 result in similar ion structures irrespective of the initial double bond position. This supports a facility in formation of two isomeric structures for the ion at *m/z* 257, yet each isomer being quite similar for these hydroxy eicosanoids.

Table 1. Hydroxy, Polyunsaturated Fatty-Acid Anions Collisionally Activated to Selected Product Ions Note: We would like to correct this table. First remove the [M-H]- from the top of column 2 and place the heading m/z. Then add [M-H]- where indicated and replace [M-H2O]- with [M-H-H2O]- and [M-H2O-CO2]- with [M-H-H2O-CO2]-.

Eicosanoid	$[M-H]^-$ Measured[1]	Drift time (ms)	CCS (N_2)	CCS (He)
5-HETE [M-H]–	319.227	4.27	185	
$[M-H-H_2O]^-$	301.217	4.25	185	
$[M-H_2O-CO_2]^-$	257.227	3.45	171	
$[M-H-H_2O-CO_2]^-$	257.227	4.43	190	
8-HETE [M-H]–	319.227	4.12	182	
$[M-H-H_2O]^-$	301.216	3.97	180	
$[M-H-H_2O-CO_2]^-$	257.227	3.45	171	
$[M-H-H_2O-CO_2]^-$	257.227	4.27	187	
11-HETE [M-H]–	319.227	4.12	182	
$[M-H-H_2O]^-$	301.216	3.97	180	
$[M-H-H_2O-CO_2]^-$	257.227	3.45	171	
$[M-H-H_2O-CO_2]^-$	257.227	4.27	187	
12-HETE [M-H]–	319.227	4.20	184	
$[M-H-H_2O]^-$	301.216	3.98	180	
$[M-H-H_2O-CO_2]^-$	257.226	3.45	171	
$[M-H-H_2O-CO_2]^-$	257.226	4.43	190	
15-HETE [M-H]–	319.227	4.13	182	
$[M-H-H_2O]^-$	301.216	4.05	181	
$[M-H-H_2O-CO_2]^-$	257.227	3.45	171	
$[M-H-H_2O-CO_2]^-$	257.227	4.43	190	
LTB_4[1,2] [M-H]–	335.222	4.28	183[3]	118
$[M-H-H_2O]^-$	317.212	4.28	185	118
$[M-H-H_2O]^-$	317.212	5.33	205	134
$[M-H-H_2O-CO_2]^-$	273.222	3.90	179	108
$[M-H-H_2O-CO_2]^-$	273.222	4.73	195	124
m/z 203.1795	203.180	2.70	158	95
m/z 195.0974	195.102	2.33	151	88

The measured exact masses, drift times, and collisional cross section (CCS) reported in Å^2

[1]Exact masses reported using the molecular anion exact mass as the lockmass

[2]CID collision energy 30 V (laboratory frame of reference)

[3]Five independent measurements were carried over a 6-month period with an average value of 182.6 ± 1.3 Å^2 (SD)

LTB_4

The collision activation of the $[M-H]^-$ from LTB_4 at *m/z* 335 yielded a large number a product ion, with the most abundant being *m/z* 195 as previously reported (Figure 3a). The proposed mechanism of formation of this ion was suggested to involve a Diels-Alder reaction with formation of a cyclic ion structure (see below) and an alkoxide anion at carbon-12 likely from a remote charge exchange with the carboxylate anion (Scheme 3) [7, 31]. This mechanism would be dependent on intramolecular folding of LTB_4 back onto itself during the process of formation of this characteristic ion.

The loss of H_2O from LTB_4 could come from three different sites: loss of a carbon-12 hydroxyl group, carbon-5 hydroxyl group, or a carboxyl oxygen atom plus two protons. In order to investigate which group was lost predominantly, the 12-hydroxyl group of LTB_4 was labeled with oxygen-18 by opening the epoxide ring of

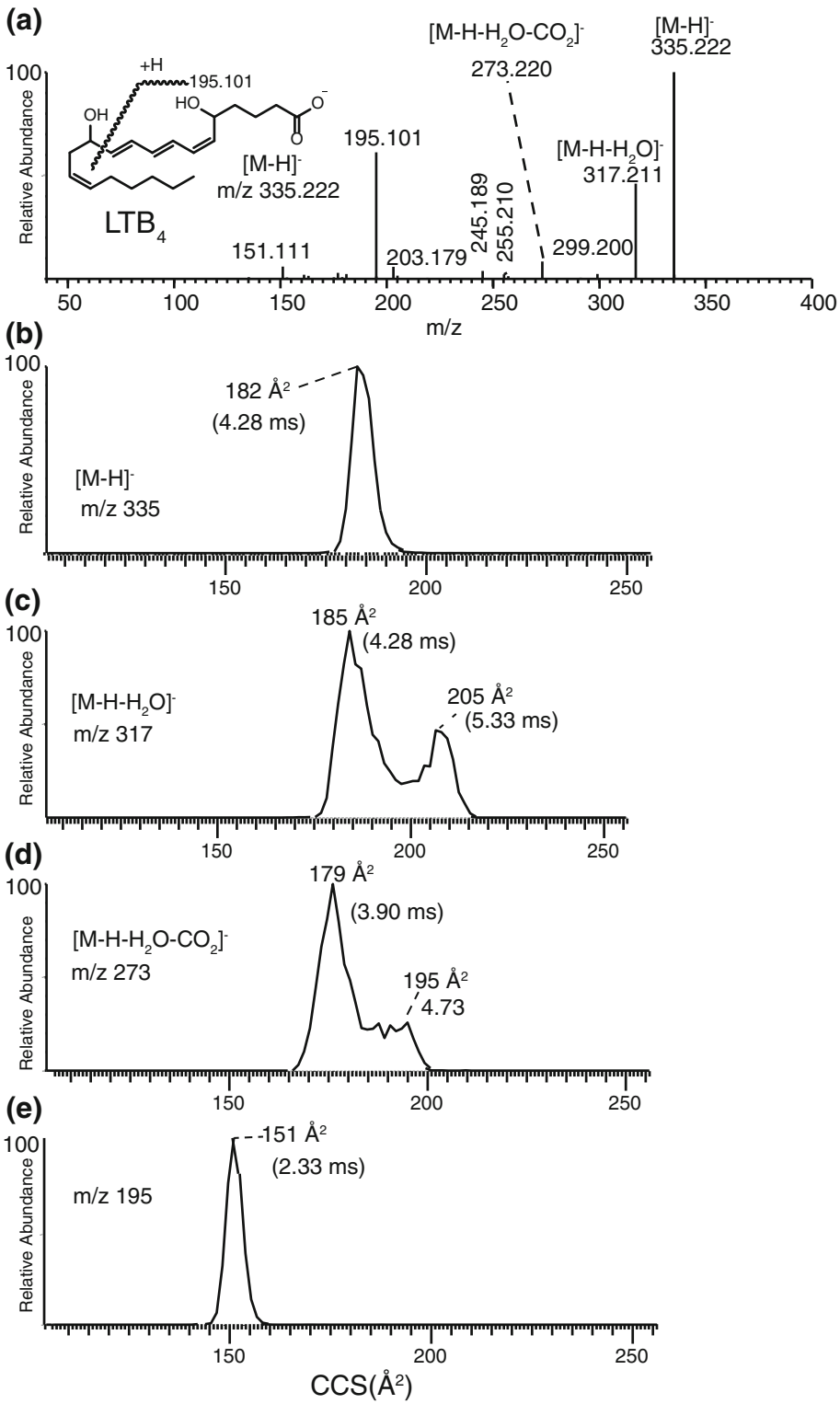

Figure 3. (a) Tandem mass spectrum of LTB_4 with 20 V applied in the collision cell. (b) Ion mobility of *m/z* 335.222 $[M-H]^-$. (c) Ion mobility of *m/z* 317.221 $[M-H-H_2O]^-$. (d). Ion mobility of *m/z* 273.220 $[M-H-H_2O-CO_2]^-$. (e) Ion mobility of diagnostic ion *m/z* 195.1. See inset structure for origin of *m/z* 195.1. The collision energy used for this mass spectrum was 20 V

LTA_4 methyl ester with $H_2{}^{18}O$. After saponification and purification of the resulting 5-hydroxy-12-[^{18}O] hydroxyl-6,8,10,14-eicosatetraenoic acid, the collisional activation of *m/z* 337 revealed that the loss of H_2O was predominantly loss of $H_2{}^{18}O$ from carbon-12 with the major ions appearing at *m/z* 317 and 273 consistent with the lack of oxygen-18 in these product ions (Supplemental Figure S5). As expected from the mechanism of formation

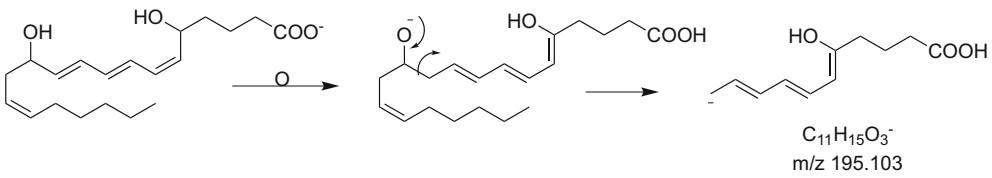

Scheme 3. Collision-induced rearrangement and mechanism of major product ion formation from LTB_4 molecular anion

(see above), the most abundant product ion *m/z* 195 also did not retain oxygen-18.

The ion mobility profiles of $[M\text{-}H]^-$ (Figure 3b) and *m/z* 195 (Figure 3d) were found to be single populations of drift times at 185 and 151 $Å^2$, respectively, but the ions corresponding to the loss of H_2O from the $[M\text{-}H]^-$ at *m/z* 317 and the loss of CO_2 and H_2O at *m/z* 273 revealed that the mechanisms leading to the formation of these dehydration product ions resulted in two,

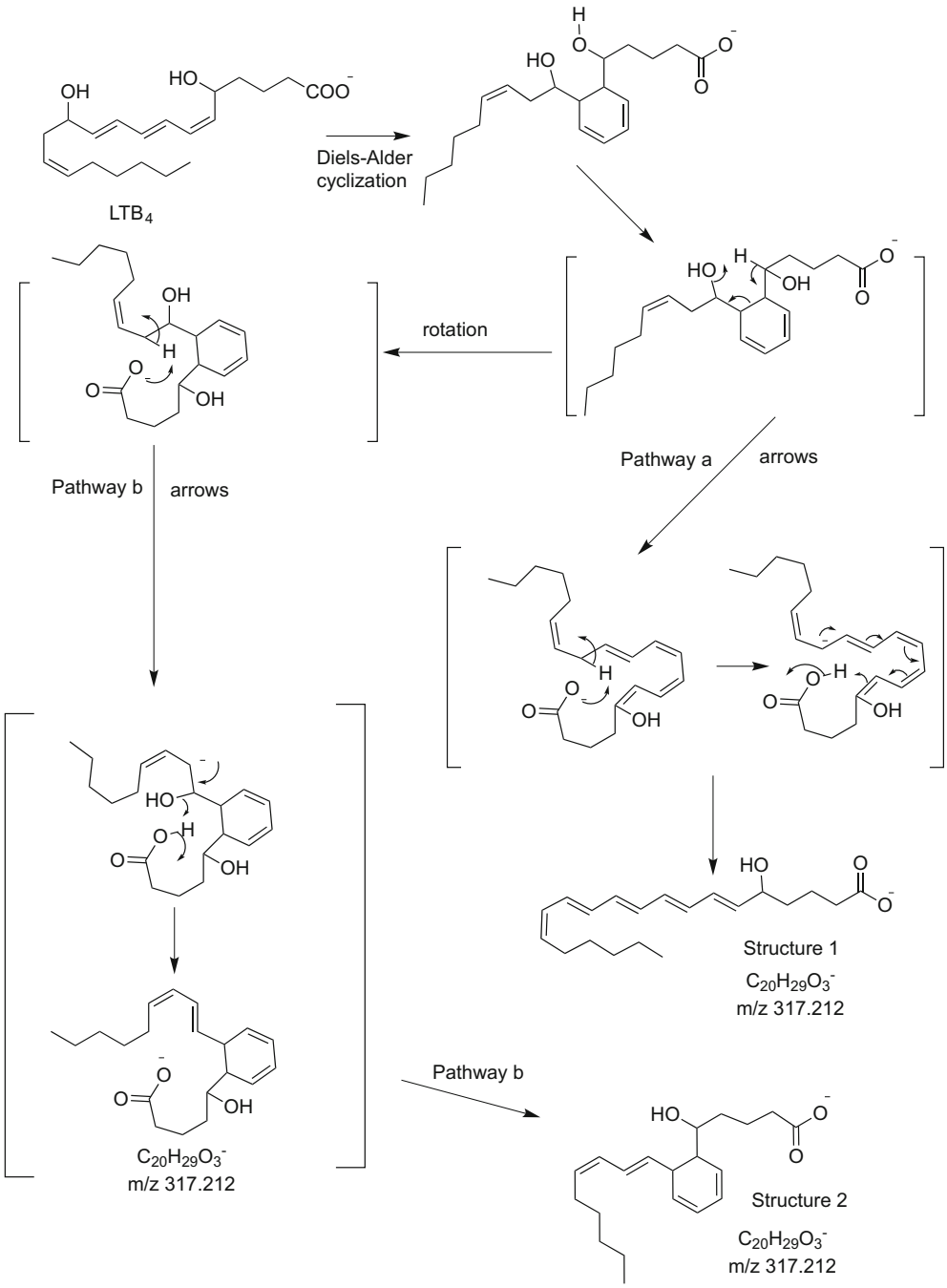

Scheme 4. Collision-induced rearrangements and two mechanisms for the formation of $[M\text{-}H\text{-}H_2O]^-$ from the LTB_4 molecular anion

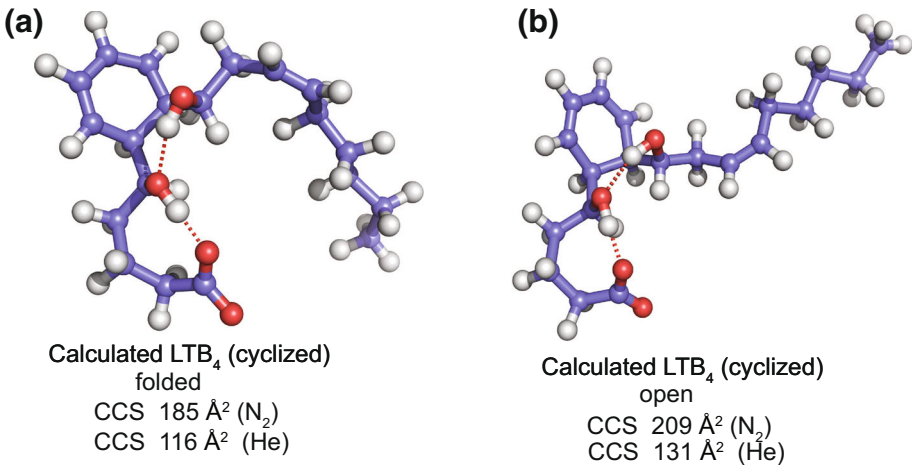

Figure 4. Molecular dynamics calculated stable structures of LTB_4 showing a hydrogen bond between the carboxylate anion (a) with the 5-hydroxyl proton and (b) with the 12-hydroxyl proton. The ion mobilities of these structures were calculated by IMos for nitrogen and helium as drift gas

quite separate ion mobilities (Table 1). This dual population of ion mobility for *m/z* 273 was more pronounced when the collisional energy in the collision cell was increased from 20 to 30 V, suggesting the higher mobility ion was formed when the energy available for collisional activation was higher (Supplemental Figure S6). Furthermore, the drift time at 4.73 ms for one population of ions at *m/z* 273 was longer than that for the precursor molecular anion $[M\text{-}H]^-$ observed at 4.28 ms. This was also the case for the ion mobilities of *m/z* 317 where the population of ions with the longest average ion mobility (5.33 ms) had a collisional cross section of 205 $Å^2$.

The loss of water from the molecular ion of LTB_4 was suggested to involve a prior Diels-Alder cyclization [17, 31] to form a cyclic intermediate of LTB_4 (Scheme 4) which facilitates the loss of H_2O from carbon-12. Such an intermediate can rearrange into either an open-chain conjugated ion structure (pathway a) or another cyclic ion (pathway b). This product ion from pathway a (Structure 1) would be predicted to have a much higher collisional cross section than the folded ion Structure 2 for *m/z* 317 $[M\text{-}H_2O]^-$. These pathways are consistent with the loss of H_2O from isotope-labeled LTB_4 isomers studied here [5-hydroxy-12-[^{18}O] hydroxy-6,8,11,14-eicosatetraenoic acid] and published ([6,7,13,14-D_4]-LTB_4) [31].

Molecular Dynamics and Collision Cross Section Calculations

Ion mobility studies of biopolymers and polymers led to the suggestion that a more folded or more compact ion three-

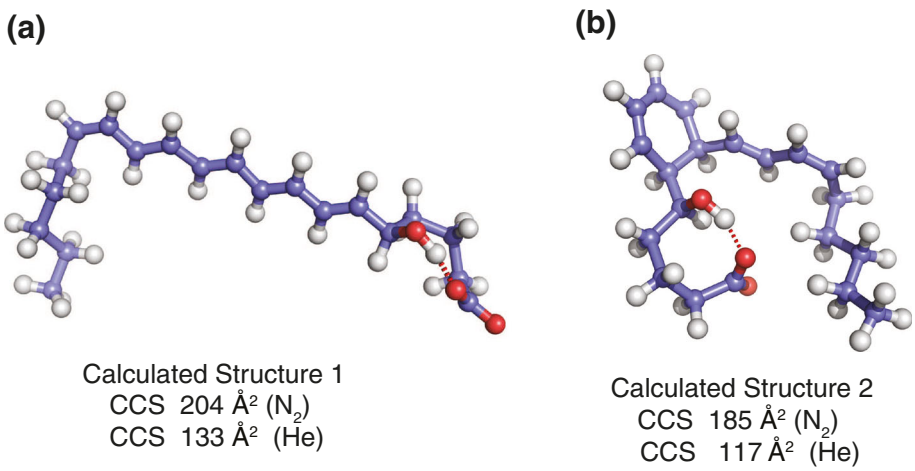

Figure 5. Molecular dynamics calculated stable structures for the ion corresponding to $[M\text{-}H\text{-}H_2O]^-$ from LTB_4 as (a) the highly conjugated, open-chain structure predicted in Scheme 4. *Pathway a* showing a hydrogen bond between the carboxylate anion and the 5-hydroxy proton. (b) The cyclic structure predicted in Scheme 4. *Pathway b* showing a hydrogen bond between the carboxylate anion with the hydroxyl proton at carbon-5. The ion mobilities of these structures were calculated using IMos version 1.06 for nitrogen and helium as drift gas

dimensional structure would have shorter drift times (lower collisional cross section) than an open structure [32, 33]. Molecular dynamics calculations were carried out starting as the typically drawn structure of LTB_4 in order to generate an energy minimized three-dimensional structure. However, the calculations of the ion mobilities were not in agreement with the measured values of collisional cross section (Table 1). Calculations of ion mobility were then carried out on the cyclized structure of LTB_4 after a Diels-Alder reaction of the conjugated triene. This is the intermediate proposed several years ago and presented in Scheme 4. Two distinct populations of structures were found in the molecular dynamics calculations and they were a folded methyl terminus of LTB_4 next to the cyclohexadiene ring (Figure 4a) which predicted populations of structures that engaged a complex hydrogen bond bridge between the carboxylate anion and the 5-hydroxy proton as well as 12-hydroxy proton (Figure 4a). This folded structure of cyclized LTB_4 was calculated to have a CCS 185 $Å^2$ in nitrogen and a CCS 116 $Å^2$ in helium, quite consistent with the observed CCS 185 $Å^2$ (N_2) and 118 $Å^2$ (He) (Table 1). The open structure (Figure 4b) had calculated ion mobilities in N_2 and He that were not in agreement with the measured values. We would therefore suggest that the intact LTB_4 molecular ions entering the ion mobility cell had likely undergone rearrangement prior to measuring the ion mobility.

The collisional cross section for the major LTB_4 product ions was also measured in both N_2 and He drift gases. Molecular dynamics calculations were carried out on the predicted covalent structures for $[M\text{-}H\text{-}H_2O]^-$ in Scheme 4 and a number of energy minimized three-dimensional structures were found to be highly stable over the calculation period. The vast majority of the predicted structures fit into two different categories, the product ion formed by pathway a, Structure 1, (Scheme 4) that retained extended conjugation, which had a molecular dynamics calculated structure shown in Figure 5a. This open-chain structure was calculated to have a CCS of 204 $Å^2$ (N_2) and 133 $Å^2$ (He), very close to one of the observed populations of $[M\text{-}H_2O]^-$ (Table 1). For the product ion *m/z* 317 formed by pathway b, Structure 2, (Scheme 4), a rather folded structure due to a stabilizing hydrogen bond between the carboxylate anion and the carbon-5 hydroxy proton (Figure 5b). The structure for this $[M\text{-}H\text{-}H_2O]^-$ variant was calculated to have a CCS of 185 $Å^2$ in N_2 and 117 $Å^2$ in He drift gas.

Conclusions

Ion mobility measurements of product ions derived from hydroxy, polyunsaturated fatty acids (anions) can display multicomponent populations of mobilities for isobaric ions. Suggested mechanisms for product ion formation of such lipids often invoke interactions of structural moieties that induce a folded confirmation. These observations and calculations of ion mobilities support the existence of distinct structural isomers formed during the collisional activation process that bring together remote sites that facilitate subsequent decomposition reactions.

Acknowledgements

The authors wish to acknowledge and thank Dr. Carlos Larriba-Andaluz (Indiana University) for the advice and providing updated parameters for IMos 1.06.

Funding Information

This work was supported by a grant from the National Institute of Environmental Health Sciences of the National Institutes of Health (ES022172) and a grant from the National Heart Lung and Blood Institute (HL117798).

References

1. Smith, W.L., Murphy, R.C.: The eicosanoids: cyclooxygenase, lipoxygenase, and epoxygenase pathways. In: Ridgeway, N.D., McLeod, R.S. (eds.) Biochemistry of Lipids, Lipoproteins and Membranes, 6th edn, pp. 260–295. Elsevier Science, Oxford (2015)
2. Smith, W.L.: Nutritionally essential fatty acids and biologically indispensable cyclooxygenases. Trends Biochem. Sci. **33**, 27–37 (2008)
3. Murphy, R.C., Gijón, M.A.: Biosynthesis and metabolism of leukotrienes. Biochem. J. **405**, 379–395 (2007)
4. Kuhn, H., Banthiya, S., van Leyen, K.: Mammalian lipoxygenases and their biological relevance. Biochim. Biophys. Acta. **1851**, 308–330 (2015)
5. Spector, A.A.: Arachidonic acid cytochrome P450 epoxygenase pathway. J. Lipid Res. **50**, S52–S56 (2009)
6. Tsikas, D., Zoerner, A.A.: Analysis of eicosanoids by LC-MS/MS and GC-MS/MS: a historical retrospect and a discussion. J Chromatogr. B Anal. Technol. Biomed. Life Sci. **964**, 79–88 (2014)
7. Murphy, R.C.: Tandem Mass Spectrometry of Lipids: Molecular Analysis of Complex Lipids. Ch. 2. Royal Society of Chemistry, London (2015)
8. Kim, H.I., Kim, H., Pang, E.S., Ryu, E.K., Beegle, L.W., Loo, J.A., Goddard, W.A., Kanik, I.: Structural characterization of unsaturated phosphatidylcholines using traveling wave ion mobility spectrometry. Anal. Chem. **81**, 8289–8297 (2009)
9. Jackson, S.N., Wang, H.Y., Woods, A.S., Ugarov, M., Egan, T., Schultz, J.A.: Direct tissue analysis of phospholipids in rat brain using MALDI-TOFMS and MALDI-ion mobility-TOFMS. J. Am. Soc. Mass Spectrom. **16**, 133–138 (2005)
10. Groessl, M., Graf, S., Knochenmuss, R.: High resolution ion mobility-mass spectrometry for separation and identification of isomeric lipids. Analyst. **140**, 6904–6911 (2015)
11. Maccarone, A.T., Duldig, J., Mitchell, T.W., Blanksby, S.J., Duchoslav, E., Campbell, J.L.: Characterization of acyl chain position in unsaturated phosphatidylcholines using differential mobility-mass spectrometry. J. Lipid Res. **55**, 1668–1677 (2014)
12. Bowman, A.P., Abzalimov, R.R., Shvartsburg, A.A.: Broad separation of isomeric lipids by high-resolution differential ion mobility spectrometry with tandem mass spectrometry. J. Am. Soc. Mass Spectrom. **28**, 1552–1561 (2017)
13. Lintonen, T.P., Baker, P.R., Suoniemi, M., Ubhi, B.K., Koistinen, K.M., Duchoslav, E., Campbell, J.L., Ekroos, K.: Differential mobility spectrometry-driven shotgun lipidomics. Anal. Chem. **86**, 9662–9669 (2014)
14. May, J.C., Goodwin, C.R., Lareau, N.M., Leaptrot, K.L., Morris, C.B., Kurulugama, R.T., Mordehai, A., Klein, C., Barry, W., Darland, E., Overney, G., Imatani, K., Stafford, G.C., Fjeldsted, J.C., McLean, J.A.: Conformational ordering of biomolecules in the gas phase: nitrogen collision cross sections measured on a prototype high resolution drift tube ion mobility-mass spectrometer. Anal. Chem. **86**, 2107–2016 (2014)

15. Giles, K., Pringle, S.D., Worthington, K.R., Little, D., Wildgoose, J.L., Bateman, R.H.: Applications of a travelling wave-based radio-frequency-only stacked ring ion guide. Rapid Commun. Mass Spectrom. **18**, 2401–2414 (2004)
16. Zhang, F., Guo, S., Zhang, M., Zhang, Z., Guo, Y.: Characterizing ion mobility and collision cross section of fatty acids using electrospray ion mobility mass spectrometry. J. Mass Spectrom. **50**, 906–913 (2015)
17. Castro-Perez, J., Roddy, T.P., Nibbering, N.M., Shah, V., McLaren, D.G., Previs, S., Attygalle, A.B., Herath, K., Chen, Z., Wang, S.P., Mitnaul, L., Hubbard, B.K., Vreeken, R.J., Johns, D.G., Hankemeier, T.: Localization of fatty acyl and double bond positions in phosphatidylcholines using a dual stage CID fragmentation coupled with ion mobility mass spectrometry. J. Am. Soc. Mass Spectrom. **22**, 1552–1567 (2011)
18. Hankin, J.A., Barkley, R.M., Zemski-Berry, K., Deng, Y., Murphy, R.C.: Mass spectrometric collisional activation and product ion mobility of human serum neutral lipid extracts. Anal. Chem. **88**, 6274–6282 (2016)
19. Sarbu, M., Vukelić, Ž., Clemmer, D.E., Zamfir, A.D.: Electrospray ionization ion mobility mass spectrometry provides novel insights into the pattern and activity of fetal hippocampus gangliosides. Biochimie. **139**, 81–94 (2017)
20. Kapron, J., Wu, J., Mauriala, T., Clark, P., Purves, R.W., Bateman, K.P.: Simultaneous analysis of prostanoids using liquid chromatography/high-field asymmetric waveform ion mobility spectrometry/tandem mass spectrometry. Rapid Commun. Mass Spectrom. **20**, 1504–1510 (2006)
21. Berry, K.A., Barkley, R.M., Berry, J.J., Hankin, J.A., Hoyes, E., Brown, J.M., Murphy, R.C.: Tandem mass spectrometry in combination with product ion mobility for the identification of phospholipids. Anal. Chem. **89**, 916–921 (2017)
22. Paglia, G., Angel, P., Williams, J.P., Richardson, K., Olivos, H.J., Thompson, J.W., Menikarachchi, L., Lai, S., Walsh, C., Moseley, A., Plumb, R.S., Grant, D.F., Palsson, B.O., Langridge, J., Geromanos, S., Astarita, G.: Anal. Chem. **87**, 1137–1144 (2015)
23. Lalli, P.M., Corilo, Y.E., Fasciotti, M., Riccio, M.F., de Sa, G.F., Daroda, R.J., Souza, G.H., McCullagh, M., Bartberger, M.D., Eberlin, M.N., Campuzano, I.D.: Baseline resolution of isomers by traveling wave ion mobility mass spectrometry: investigating the effects of polarizable drift gases and ionic charge distribution. J. Mass Spectrom. **48**, 989–997 (2013)
24. Jakalian, A., Jack, D.B., Bayly, C.I.: Fast, efficient generation of high-quality atomic charges. AM1-BCC model: II. Parameterization and validation. J. Comput. Chem. **23**, 1623–1641 (2002)
25. Pettersen, E.F., Goddard, T.D., Huang, C.C., Couch, G.S., Greenblatt, D.M., Meng, E.C., Ferrin, T.E.: UCSF Chimera—a visualization system for exploratory research and analysis. J. Comput. Chem. **25**, 1605–1612 (2004)
26. Hinsen, K.: The molecular modeling toolkit: a new approach to molecular simulations. J. Comput. Chem. **21**, 79–85 (2000)
27. Larriba, C., Hogan, C.J.: Free molecular collision cross section calculation methods for nanoparticles and complex ions with energy accommodation. J. Comput. Phys. **251**, 344–363 (2013)
28. Larriba-Andaluz, C., Hogan Jr., C.J.: Collision cross section calculations for polyatomic ions considering rotating diatomic/linear gas molecules. J. Chem. Phys. X. **141**, 194107 (2013)
29. Wheelan, P., Zirrolli, J.A., Murphy, R.C.: Low-energy fast atom bombardment tandem mass spectrometry of monohydroxy substituted unsaturated fatty acids. Biol. Mass Spectrom. **22**, 465–473 (1993)
30. Duez, Q., Josse, T., Lemaur, V., Chirot, F., Choi, C.M., Dubois, P., Dugourd, P., Cornil, J., Gerbaux, P., De Winter, J.: Correlation between the shape of the ion mobility signals and the stepwise folding process of polylactide ions. J. Mass Spectrom. **52**, 133–138 (2017)
31. Wheelan, P., Zirrolli, J.A., Murphy, R.C.: Negative ion electrospray tandem mass spectrometric structural characterization of leukotriene B_4 (LTB_4) and LTB_4-derived metabolites. J. Am. Soc. Mass Spectrom. **7**, 129–139 (1996)
32. Shvartsburg, A.A., Hudgins, R.R., Dugourd, P., Jarrold, M.F.: Structural elucidation of fullerene dimers by high-resolution ion mobility measurements and trajectory calculation simulations. J. Phys. Chem. A. **101**, 1684–1688 (1997)
33. Vonhelden, G., Wyttenbach, T., Bowers, M.T.: Inclusion of a MALDI ion source in the ion chromatography technique: conformational information on polymer and biomolecular ions. Int. J. Mass Spectrom. **146**, 349–364 (1995)